



## Computer Aided Diagnosis in Digital Mammograms: Detection of Microcalcifications by Meta Heuristic Algorithms

K.Thangavel<sup>1</sup>, M.Karnan<sup>2\*</sup>

1: Department of Mathematics, Gandhigram Rural Institute-Deemed University,

2: Department of computer science, Gandhigram Rural Institute-Deemed University,  
Gandhigram-624302, Tamil Nadu, India. Email: [karnanme@yahoo.com](mailto:karnanme@yahoo.com) fax:91-4551-227229

### Abstract

This research applies the meta-heuristic methods such as Ant Colony Optimization (ACO) and Genetic Algorithm (GA) for identification of suspicious region in mammograms. The proposed method uses the asymmetry principle (bilateral subtraction): Strong structural asymmetries between corresponding regions in the left and right breast are taken as evidence for the possible presence of microcalcification in that region. Bilateral subtraction is achieved in two steps. First, the mammogram images are enhanced using median filter, pectoral muscle region is removed and the border of the mammogram is detected for both left and right images from the binary image. The enhancement technique is evaluated by signal to noise ratios. Further GA is applied to enhance the detected border. The figure of merit is calculated to identify whether the detected border is exact or not. And the nipple position is identified for both left and right images using GA and ACO, and their performance is studied. Second, using the border points and nipple position as the reference the mammogram images are aligned and subtracted to extract the suspicious region. Results obtained with a set of mammograms indicate that this method can improve the sensitivity and reliability of the systems for automated detection of breast tumors i.e. microcalcification. The algorithms are tested on 161 pairs of digitized mammograms from Mammographic Image Analysis Society (MIAS) database. A Free-Response Receiver Operating Characteristic (FROC) curve is generated for the mean value of the detection rate for all the 161 pairs of mammograms in MIAS database, to

evaluate the performance of the proposed method.

**Keywords:** Breast boarder, nipple identification, genetic algorithm, ant colony optimization, bilateral subtraction. FROC.

### 1 Introduction

Breast cancer is one of the leading cancers in the female population. About 25% of all cancers diagnosed in women are breast cancers and about 20% of all lethal cancers are breast cancers. It is the leading cause of death due to cancer in women [11]. The risk of developing Breast Cancer can be reduced by: Having children before 30, Breast-feeding, Limiting alcohol intake, maintaining a healthy weight, exercising regularly.

X-ray mammography is the most effective imaging technique for the early-diagnosis of breast cancer. Mammography-based screening programs are carried out in many countries, and their effectiveness has had a great impact on prognoses. A mammographic image is characterized by a high spatial resolution that is adequate enough to detect subtle fine-scale signs such as microcalcifications. On the other hand, the analysis of mammographic images is a complex and cumbersome task that requires highly specialized radiologists. In addition, population screening produces a very large number of images, most of which are usually negative. The performance of the observer can be degraded by the huge resulting caseload, which is undoubtedly caused by visual fatigue and other psychophysical mechanisms. Double readings, as carried out, for example, by two radiologists, usually improve the quality of diagnostic findings, thus, greatly reducing

the probability of misdiagnosis. On these grounds, adequate computational tools are expected to be helpful to the radiologist. Thangavel et al., [57] and Cheng et al., [8] are presented a study on methods of various stages on automatic detection of microcalcification in digital mammograms. According to those studies it is noted that the Ant Colony Optimization (ACO) has not been implemented in the field of mammogram analysis. In this paper, metaheuristic algorithms such as GA and ACO are implemented to extract the suspicious region based on asymmetry approach.

#### ***Overview and Merits of Metaheuristic Algorithms:***

Recently, many researchers have focused their attention on a new class of algorithms, called metaheuristics. A metaheuristic is a set of algorithmic concepts that can be used to define heuristic methods applicable to a wide set of different problems. In other words, a metaheuristic can be seen as a general-purpose heuristic method designed to guide an underlying problem specific heuristic toward promising regions of the search space containing high-quality solutions. A metaheuristic therefore a general algorithmic framework, which can be applied to different optimization problems with relatively few modifications to make them, adapted to a specific problem. The use of metaheuristics has significantly increased the ability of finding very high-quality solutions to hard, practically relevant combinatorial optimization problems in a reasonable time. This is particularly true for large and poorly understood problems. Several meta-heuristics, such as genetic algorithms [24,33], tabu search [23] and simulated annealing [37], have been proposed to deal with the computationally intractable problems. Ant colony optimization (ACO) is a new metaheuristic developed for composing approximate solutions. The ant algorithm was first proposed by Colormi et al., (1991) and has been receiving extensive attention due to its successful applications to many combinatorial optimization problems [10,14]. Like genetic algorithm and simulated annealing approaches, the ant algorithms also foster its solution strategy through use of nature metaphors. The ACO is based upon the behaviors of ants that they exhibit when looking for a path to the advantage of their colony. Unlike simulated annealing or tabu search, in which a single agent is deployed for a single beam session, ACO and genetic algorithms use multiple agents, each of which

has its individual decision made based upon collective memory or knowledge. Recently, the ACO metaheuristic has been proposed to provide a unifying framework for most applications of ant algorithms [13,15] to combinatorial optimization problems. Algorithms that actually are instantiations of the ACO metaheuristic will be called ACO algorithms [2,16,19,22,27,49]. This paper presents an automatic alignment for analyzing corresponding mammogram images using genetic algorithm and ant colony optimization technique.

***Overview of Genetic Algorithm:*** A genetic algorithm is an iterative procedure that involves a population of individuals, each one represented by a finite string of symbols, known as the genome, encoding a possible solution in a given problem space [12,45,50]. This space, referred to as the search space, comprises all possible solutions to the problem at hand. The standard genetic algorithm proceeds as follows: an initial population of individuals is generated at random or heuristically. Every evolutionary step, known as a generation, the individuals in the current population are decoded and evaluated according to some predefined quality criterion, referred to as the fitness, or fitness function. To form a new population, individuals are selected according to their fitness. Thus, high-fitness individuals stand a better chance of ‘reproducing’, while low-fitness ones are more likely to disappear. Then crossover is performed with the probability  $p_c$  between two selected individuals, called parents, by exchanging parts of their genomes to form two new individuals, called offspring. Next, the mutation operator is introduced to prevent premature convergence to local optima by randomly sampling new points in the search space. Flipping bits at random carries it out; with some small probability  $p_m$ . Genetic algorithms are stochastic iterative processes that are not guaranteed to converge. The termination condition may be specified as some fixed, maximal number of generations or as the attainment of an acceptable fitness level.

***Overview of Ant Colony Optimization:*** Ant Colony Optimization (ACO) metaheuristic; a recent population-based approach, is inspired by the observation of real ants colony and based upon their collective foraging behavior [16,49]. Real ants are capable of finding the shortest path from a food source to the nest without using visual cues [1,27]. Ants are moving on a straight line that connects a food source to their nest is a pheromone trail. Pheromone is a volatile chemical substance lay down by ants while walking, and each ant probabilistically prefers to follow a direction rich in

pheromone. This elementary behavior of real ants can be used to obtain optimum value from a population. In ACO, solutions of the problem are constructed within a stochastic iterative process, by adding solution components to partial solutions. Each individual ant constructs a part of the solution using an artificial pheromone, which reflects its experience accumulated while solving the problem, and heuristic information dependent on the problem [2,19,22].

Two different techniques are used in the interpretation of mammograms. The first technique consists of a systematic search of each mammogram for visual patterns symptomatic of tumors. Such as, a bright, approximately circular blob with hazy boundary might indicate the presence of a circumscribed mass [39,56]. The second technique, the asymmetry approach, consists of a systematic comparison of corresponding regions in the left and right breast. Significant structural asymmetries between the two regions can indicate the possible presence of a tumor. Most researchers have focused on processing a single image to find abnormalities. In comparison, only a handful of researchers have dealt with analysis of bilateral mammograms [3,30,35,36,41,46,60,62,63,64] and even fewer have dealt explicitly with comparing time sequences of mammograms [5,20,29,41,52,55,59,65].

This paper follows the asymmetry approach to extract the suspicious region in mammograms. The technique presented in this paper is applicable to bilateral and time sequences of mammograms. However, only bilateral mammograms are used in the evaluation since large data sets of bilateral images are more readily available. The technique is fully automated and it recovers deformations that go beyond simple translation, scale and rotation. The reason for considering this approach is, methods that attempt to detect specific tumors, are likely to give a better performance, however, the method presented here can provide clues about the presence of tumors that are not available to other methods and thus it provides another building block for a clinically useful system. The strategy of the asymmetry detection system can be described as follows: Given a pair of identical-view mammograms of the left and right breast, detect all structural asymmetries between corresponding positions in the left and right breast. Significant asymmetries are taken as evidence for the possible presence of a tumor.

In this proposed method, the combination of genetic operators (reproduction, crossover, mutation) is applied to detect the border of the mammogram image. To identify the nipple on digital mammograms a novel method, Ant Colony Optimization and Genetic Algorithm are implemented, and compared. Using the border coordinates and nipple position of left and right mammograms, the images are aligned and subtracted to extract the suspicious regions. Prior to bilateral subtraction, the pectoral muscle region is removed from the breast region and the mammogram images are normalized.

The following section presents an overview of the proposed method. Section 2 explores preprocessing and enhancement techniques such as median filtering, removal of pectoral muscle and normalization for mammogram images. Section 3 presents genetic algorithm for breast boarder detection. Section 4 presents the nipple identification techniques using genetic algorithm and Ant Colony Optimization. The alignment of mammograms and generating asymmetry image are described in Section 5. The experiments and results are presented in Section 6. And Section 7 describes the conclusion.

## 1.1 Overview Of The CAD System

A closer inspection of the mammograms reveals several difficulties for the asymmetry approach. First, the global appearance (brightness, contrast, etc.) of the two breasts may differ, usually due to variations in the recording procedure. In this work, initially the mammogram images are enhanced by median filter to remove the high frequency components (ie.noise) from the image. Then the pectoral muscle region is eliminated. Second, due to natural asymmetry, and due to the mammographic recording procedure, the shapes of the left and right breast do not match. Defining corresponding positions in both breasts becomes therefore a nontrivial task. The breast border and the nipple position of the mammogram are detected to find the deflection between both left and right mammograms.

In border detection, the mammogram image is converted into binary image [55]. From the binary image the border points are extracted and it is mapped with the original image. The extracted border is enhanced using genetic algorithm as follows: From the extracted border, for each border points a 3×3-window size of neighborhood pixels (kernel) are taken, and they are considered as initial population for genetic algorithm. The sum of intensity values of all the pixels in a kernel is

considered as fitness values for the kernel. The genetic operators like reproduction, crossover, and mutation are applied to the kernels. The kernels from the final population has the enhanced border pixels, they are mapped with the original image. Next step is to find out the nipple position of the mammogram image. A genetic algorithm and a novel method; Ant Colony Optimization is used to identify the nipple position and the results are compared.

The border points are considered as the population for both GA and ACO algorithms to identify the nipple position. In GA, the genetic operators, reproduction, crossover and mutation are applied on border points to generate the new population at each iteration. The minimum value is calculated from the final population at final iteration. This minimum value is compared with the intensity values of the border points. The matching pixel is considered as the nipple

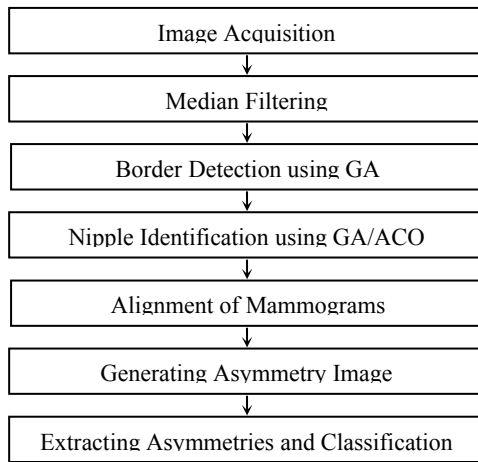


Figure 1. Block Diagram for Extracting Suspicious Region from Background Tissue

position. In the case of ACO, the ants start their search from a random border point with initial pheromone value. Then the Maximizing A Posterior (MAP) function is evaluated for each ant, and the pheromone values are updated for each ant. The global minimum value is calculated at the end of each iteration. The border pixel, whose intensity value is equal to the global minimum value from the final iteration, is considered as the nipple position. The coordinate points of border points and nipple position of both left and right images are compared to find out the deflection between two images. Then the right image is aligned to correspond with the left image. Then the left and right images are subtracted to extract the suspicious region. Figure. 1 shows that the

methods employed in the proposed method for extraction of suspicious region.

## 2 Preprocessing and Enhancement

Image enhancement refers to attenuation, or sharpening, of image features such as edges, boundaries, or contrast to make the processed image more useful for analysis. Image enhancement includes gray-level and contrast manipulation, noise reduction, background removal, edge crisping and sharpening, filtering, interpolation and magnification, pseudo-coloring, and so on. The greatest difficulty in image enhancement is quantifying the evaluation criteria for enhancement. Image enhancement techniques can be improved if the enhancement criteria can be stated precisely. Often such criteria are application dependent. This section presents the preprocessing and enhancement procedures such as median filtering, normalization and removal of pectoral muscle region for enhancement of mammograms. The performance of the enhancement technique is evaluated by Signal to Noise Ratio (SNR).

### 2.1 Median Filtering

Median filtering has been found to be very powerful in removing noise from two-dimensional signals without blurring edges. This makes it particularly suitable for enhancing mammogram images [44]. To apply median filtering to a mammogram, the low-frequency image was generated by replacement of the pixel value with a mean pixel value computed over a square area of 11x11 pixels centered at the pixel location [39,53]. The pre-processing phase is the most important step in image analysis and the classification result will depends on the preprocessing result. The evaluation criteria for median filtering is considered as follows:

**Performance evaluation:** Li et al. [42,43] used Contrast, Contrast Improvement Index (CII), background noise level, Peak Signal-to-Noise Ratio (PSNR), and Average Signal-to-Noise Ratio (ASNR) to evaluate the enhancement performance [40]. The definitions of contrast and CII are defined as,

$$CII = C_{\text{processed}} / C_{\text{original}}, \quad (1)$$

where  $C_{\text{processed}}$  and  $C_{\text{original}}$  are the contrasts for a mammogram in the processed and original images, respectively. The contrast  $C$  of a region is defined by

$$C = (f - b) / (f + b) \quad (2)$$

where  $f$  is the mean gray-level value of the foreground and  $b$  is the mean gray-level value of the background. The background noise level is

measured by the standard derivation  $\sigma$  of the background:

$$\sigma = \sqrt{(1/N) \sum_i (b_i - b)^2}, i=1, \dots, N \quad (3)$$

where  $b_i$  is the gray-level value of a surrounding background region, and  $N$  is the total number of pixels in the surrounding background region. PSNR and ASNR are defined as follows:

$$\begin{aligned} \text{PSNR} &= (p - b) / \sigma; \text{ and} \\ \text{ASNR} &= (f - b) / \sigma \end{aligned} \quad (4)$$

where  $p$  is the maximum gray-level value and  $f$  is the average gray-level value of a foreground. The values of the two indexes are larger, the enhancement method performance better.

## 2.2 Normalization of mammograms

Mammogram images are corrected to avoid differences in brightness between the left and right mammograms caused by the recording procedure [7]. The Figure 2 shows the original and normalized mammogram. In order to reduce the variation, and achieve computational consistency, the images are normalized, by mapping all mammograms into a fixed intensities range  $r1$  and  $r2$  ( $0 \leq r1 < r2 \leq 255$ ). Assume an image  $g_i(x,y)$  whose maximum gray level is  $\max G_i$  and minimum gray level is  $\min G_i$ , transform  $g_i(x,y)$  into  $g_k(x,y)$

$$g_k(x,y) = \{r1 + (g_i(x,y) - \min G_i) \times (r2 - r1)\} / \{\max G_i - \min G_i\} \quad (5)$$

In this work,  $r1$  and  $r2$  are assigned with the values 60 and 210 respectively [7], due to the fact that maximum intensities and minimum intensities of the microcalcifications are not beyond  $r2$  and below  $r1$  with certainty after investigating a huge amount of mammograms.

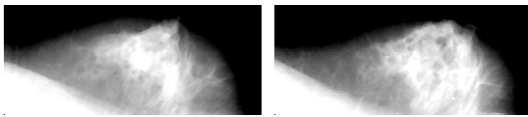


Figure 2. Normalized Mammogram Images

## 2.3 Pectoral Muscle Extraction

The reliability of boundary matching may be increases by extracting the pectoral muscle from the breast region. The pectoral muscle appears as a bright triangular region in the image corner towards the chest wall and the bottom of the breast region. A histogram-based thresholding technique is used to separate the pectoral muscle region. The global optimum in the histogram is selected as the threshold value. The intensity values smaller than this threshold are changed to black (0), and the gray values greater than the

threshold are changed to white (1). The erosion and dilation operators are used to better preserve the pectoral muscle region. Then the gray level mammogram image is converted to binary image to segment the pectoral muscle region. The white pixels in the lower left corner of the mammogram image indicate the pectoral muscle region. The corresponding white pixels in the segmented breast region image are changed to black (0) to remove the pectoral muscle region from the breast region. Figure 3 shows the breast region of left and right mammograms after the removal of pectoral muscle region.

In processing mammogram views known to contain

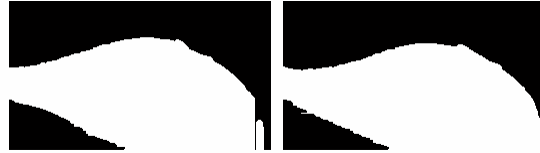


Figure 3. Removal of Pectoral Region

a pectoral muscle, the following algorithm attempts to remove the pectoral muscle region from the breast region [55]. If only a small portion of the muscle is visible in the image the algorithm simply matches the full breast region outline for the images being compared [20,21,38].

### Algorithm: Removal of Pectoral Muscle Region

---

```

S (5) Read the mammogram image
[m n] ← size of the image
th ← peak threshold value from the histogram
for each pixel in Sij { i=1,..m; j=1,..n }
  if (Sij < th)
    Bij = 0;
  else
    Bij = 1;
end
Bij ← erosion (Bij)
Bij ← dilation (Bij)
for each pixel in Bij
  if (Bij = 1)
    Sij = 0
  end
end
Sij ← image after the removal of pectoral muscle
region
```

---

## 3 Breast Border Detection

Segmentation of the breast region and non-breast region is a necessary prerequisite for further bilateral subtraction. This section presents the border detection method using genetic algorithm. The breast border can be obtained by segmenting the

breast region in the image. Some authors have developed methods to identify the breast region on the basis of a global histogram analysis [41,62,63]. However, a method based on global thresholding alone is critically dependent on the selection of the threshold values. Bick et al. [4] developed a method on the analysis of the local gray-value range to classify each pixel in the image. Clarke et al., [9] and Qian et al., [54] have developed a segmentation algorithm based on wavelet transformation. Wirth and Stapinski [61] have explored the application of active contours to the problem of extracting the breast region in mammograms.

### 3.1 Existing Methods

Mendez et al., [44] developed a fully automatic technique to detect the breast border and the nipple. First, a smoothed version of the threshold image is generated. Five reference points,  $(x_1, y_1)$ ,  $(x_2, y_2)$ ,  $(x_3, y_3)$ ,  $(x_4, y_4)$  and  $(x_5, y_5)$ , are automatically selected dividing the breast into three regions. Finally, a tracking algorithm [44] detects the border establishing that a point  $(x_i, y_i)$  belongs to the breast border if the gray level value  $f(x, y)$  of its nine previous pixels verifies the condition:

$$\begin{aligned} f(x_1, y_1) < f(x_2, y_2) < \dots < f(x_7, y_7) \leq f(x_8, y_8) \leq \\ f(x_9, y_9) \leq f(x, y) \end{aligned} \quad (6)$$

The detection algorithm was relaxed such that the breast border obtained was always external to the real border. Calculating the slope of the breast border in the reference points  $(x_1, y_1)$  and  $(x_2, y_2)$ , the detected border was enlarged until it reached the edge of the digital image. Hence, the breast region where the relevant information for diagnosis is included was completely determined within a closed contour.

Chandrasekhar and Attikiouzel [6] developed a simple method for detecting the breast border. Initially, histogram equalization is applied to the mammogram image, and then intensity change is applied to each original intensity value,  $I_0$ , to yield the new intensity,  $I_n$ , which is given by;

$$I_n = (mI_0) \bmod 256, \quad (7)$$

where,  $m$  is the number of cycles to be performed. The gray level mammogram is converted to binary image [55], showing the breast and background. A threshold value ( $T$ ) is assigned with the peak value from the histogram of the mammogram image. The intensity values are changed as

$$\text{if } A(x, y) < T, B(x, y) = 0; \text{ else } B(x, y) = 1, \quad (8)$$

where  $A$  is the original image and  $B$  is the binary image. The binary image is searched from top to bottom, a point  $(x, y)$  would belong to the border

$$\text{if } B(x, y) = 1 \text{ and } B(x-1, y) = 0; \quad (9)$$

the points those satisfies the above conditions are stored as border pixels.

Also mammogram images can be enhanced by logarithmic transformation, and morphological operations are performed to extract the breast border. First, the logarithmic transformation [18,27] function is used to enhance the mammogram image. Histogram-based thresholding technique is used to separate the breast region and non-breast region. Histogram is generated for the mammogram image. The peak point of the histogram is select as the threshold value ( $T$ ).

$$\text{If } g(x, y) < T, b(x, y) = 0, \text{ else } b(x, y) = 1, \quad (10)$$

where  $g$  is the original image and  $b$  is the binary image [34,51]. The interior pixels inside the segmented breast regions are removed using erosion and then dilation operations with octagonal-shaped operators. Once the interior pixels are removed, the binary image only contains the border pixels alone as white pixels. The spatial coordinate points of these white pixels can be mapped with the gray level mammogram. To draw the border, the corresponding pixels are set to 255, i.e., white pixels.

In this paper the genetic algorithm is used to detect the breast boarder. A histogram-based thresholding technique is used to separate the dark background region. The local optimum in the histogram is selected as the threshold value. The intensity values smaller than this threshold are changed to black (0), and the gray values greater than the threshold are changed to white (1). The segmented foreground regions are processed using morphological operations [32] with octagonal-shaped operators of radius 21. The octagonal shape is used to better preserve the shape of the anterior part of the breast boundary. The obtained breast border points are mapped with the original gray scale mammogram image.

By using the edge map as a solution space for the GA, no special mappings are required, small neighborhood windows can be overlaid, and edge structures and pixels can be modified on a local, intuitive basis. Furthermore, this representation allows for easy transition into an extended type of chromosome for the GA, the kernel, defined as an array of bits instead of the conventional bit vector, or string, used in traditional GA's. A kernel is highly

compact memory usage, essential when running a simulation with a large population, or a large image.

### 3.2 Detection of the breast border using Genetic Algorithm

A Genetic Algorithm (GA) is an optimization technique for obtaining the best possible solution in a vast solution space. Genetic algorithms operate on populations of strings, with the string coded to represent the parameter set. Genetic algorithm consists of three operators such as reproduction, crossover and mutation. These operators are applied to successive string populations to create new string populations.

Reproduction is a process that selects the members from the population for crossover. This operator is implemented by roulette wheel where each string in the population has a roulette wheel slot sized in proportion to its fitness. A simple spin of the weighted roulette wheel yields the reproduction string. In crossover, random number of bits is exchanged between the newly reproduced strings. Mutation is the occasional random alteration with small probability of the value of the string position; this simply means changing 1 to 0 and vice versa. The process of generating new population is iterated till, either a sufficiently good solution is found, or after a predetermined number of iterations [25,26,28,45,58].

Border detectors normally represent edges in a binary image, where each pixel takes on either the intensity value zero for a non-border pixel or one for a border pixel. Each pixel in the binary map corresponds to an underlying pixel in the original image. In this proposed system a kernel is defined as a neighborhood array of pixels with the size of  $3 \times 3$  window instead of the conventional bit vector, or string, which is essential when running a simulation with a large population, or a large image.

The corresponding kernels are extracted from gray level mammogram image using spatial coordinate points, and the intensity values of the pixels in the kernel are summed and this sum is considered as fitness values. After the initial population is generated, genetic operators can be applied in this population to generate the new one. Reproduction operator produces a new string for crossover. Reproduction is implemented as linear search through roulette wheel with slots weighted in proportion to kernel

fitness values. In this function, a random number multiplies the sum of the population fitness, called as stopping point. The partial sum of the fitness value is accumulated in a real variable until it is greater than or equal to the stopping point. The location where the iteration stops, the corresponding kernel is selected for crossover. The newly reproduced kernels are crossed over by exchanging the values in the window with the size of  $2 \times 2$ . Figure 4 shows the cross over operation. The kernels A and B are from old population, and X and Y are the kernels after crossing over.

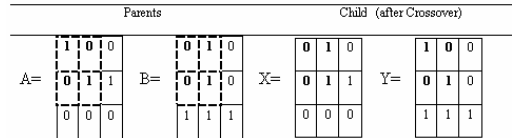


Figure 4. Crossover Operator

Next, the mutation operator is introduced to prevent premature convergence to local optima by

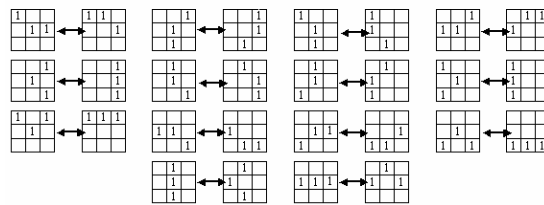


Figure 5. Mutation Operator

randomly sampling new points in the search space. Flipping bits at random carries it out, with some small probability. When mutation occurs on a bit string representation, the bit corresponding to the gene to be mutated is flipped or flopped, i.e., its value is changed from 0 to 1 or vice versa. In mutation, if a border configuration that matches one of the 28 configurations in Figure 5 is found, the corresponding transformation is performed. If the edge configuration at this site does not correspond to any of those, no change is made. The new kernels are stored as new population. This procedure is performed until the size of the new population is equal to the initial population. Then the old population is assigned with new population value and the same procedure is performed again to generate the next population. Finally, the kernels in the latest population have the enhanced border points. They can be mapped with the original image. Figure 6 shows the breast border extracted using genetic algorithm.

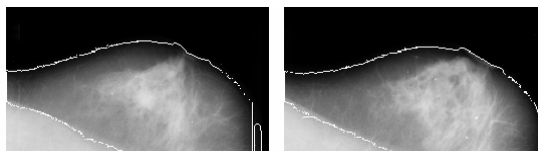


Figure 6. Border Detection Using Genetic Algorithm

**Performance Evaluation:** The performance of the detected border using genetic algorithm is tested with Pratt's figure of merit. The Pratt's figure of merit [51] can be used to quantitatively compare the results of different edge detectors. It measures the deviation of the output edge from a known ideal edge in the following manner [39]:  

$$P = (1 / \max(I_A, I_I) \sum_i (1 / (1 + \alpha d^2(i))))$$
,  $I = 1, \dots, I_A$  (11)  
 where,  $I_A$  is the number of edge points detected,  $I_I$  is the number of edge points in the ideal edge image,  $\alpha$  is a scaling factor, and  $d(i)$  is the distance of the detected edge pixel from the nearest ideal edge position. Pratt's figure of merit is a rough indicator of edge quality. A higher value for the Pratt figure of merit denotes a better edge image. Gudmundsson et al., [28] developed an edge detection algorithm using Simulated Annealing (SA); the value of  $P$  for this method is 0.83, and Mendez et al., [44] achieves only 0.89, whereas the proposed GA approach produces 0.93, which shows that the genetic algorithm can detect the breast border better.

**Algorithm:** Detection of Breast Border using Genetic Algorithm

---

$S_{ij} \leftarrow$  Original Image;  $B_{ij} \leftarrow$  Border image  
 $[m \ n] \leftarrow$  size of  $B_{ij}$   
**for** each border pixel in  $B_{ij}$   
 $K \leftarrow$  kernel of the border pixel of size  $3 \times 3$   
 $F \leftarrow$  fitness value; sum of the intensity values of all the pixels in a kernel  
 $Pop1 \leftarrow$  initial population contains  $K$  and  $F$   
**end**  
**repeat** for  $N$  times  
     **for** each string in  $Pop1$   
          $k1, k2 \leftarrow$  select two kernels for reproduction.  
 For the selection of two kernels roulette wheel is implemented as follows:  
 (i)  $r = \text{random}() * \text{sum\_of\_fitness}$   
     [Hint:  $\text{random}()$  function returns a random number between 0 and 1]  
 (ii)  $\text{partsum} = 0$ ,  $i = 0$ ,  $m \rightarrow$  size of the population  
 (iii)  $p \rightarrow$  contains the population strings  
 (iv)  $\text{partsum} = \text{partsum} + p(i)$   
 (v)  $i = i + 1$   
 (vi) **if** ( $i \leq m$ ) and ( $\text{partsum} < r$ ) Goto Step:  
     (iv) **else** return  $i$   
 $k3, k4 \leftarrow$  new kernels after crossover.  
 $k5, k6 \leftarrow$  kernels after mutation, here a random bit in the kernel is flipped or flopped. In mutation, if a border configuration that matches

one of the 28 configurations in Figure 5 is found, the corresponding transformation is performed.

$Pop2(p) \leftarrow k5$ ;  $p \leftarrow p+1$ ;  $Pop2(p) \leftarrow k6$ ;  
**end**  
 $Pop1 \leftarrow Pop2$ ;  
 Map the kernels with the  $B_{ij}$   
**end**

---

## 4 Identification of The Nipple Position

The nipple may appear either in profile or not in profile. The nipple is located on the mammogram close to where the rate of change among gray-levels is larger than in the rest of the breast. This section presents two algorithms, using genetic algorithm and Ant Colony Optimization, for identifying the nipple position.

### 4.1 Existing Methods

Mendez et al., [44] developed a gradient method, the maximum height of the breast border is taken as the position of the nipple. The maximum of the gradient across the median-top section of the breast was calculated over a straight line connecting a point at the border ( $x_b, y_b$ ) and a reference point inside the mammogram. The average intensity gradient method is used for automatically locating the nipple on digitized mammograms that have been segmented to expose the skin-air interface [6]. If the average gradient of the intensity is computed in the direction normal to the interface and directed inside the breast, it is found that there is a sudden and distinct change in this parameter close to the nipple. Specifically, the nipple is located midway between a successive maximum and minimum of the derivative of the average intensity; these being local turning points for a nipple in profile and global otherwise. The maximum of the second derivative was calculated over straight lines connecting each point of the border with a reference point inside the breast, was taken as the position of the nipple. In this case, the result is dependent not only on the gray-level at both the center ( $x, y$ ) and the border ( $x_b, y_b$ ), but also the shape of the straight line [44].

### 4.2 Identification of Nipple Position using Genetic Algorithm

Initially the breast is divided into three regions [44]. The intensity values of the border pixels in the second region are considered as initial population for the genetic algorithm [58]. The intensity values of the border points are then converted as binary strings, and these values are considered as population strings for genetic algorithm. Now the

genetic operators such as reproduction, crossover, and mutation are applied to get new population of strings [17,18,20,26]. Finally, the border pixel, which generates the minimum value of the population, is considered as the nipple position. The algorithm for identification of the nipple position in mammogram image using genetic algorithm is as follows:

**Algorithm:** Identification of Nipple Position using Genetic Algorithm

---

```

Sij ← Original Image; Bij ← Border image;
[m n] ← size of Bij
for each border pixel in Bij
G ← intensity of the border pixel from S,
    converted to binary string
F ← fitness value; intensity values of the pixels
Pop1 ← initial population contains G
end
p ← 1
repeat for N times
    for each string in Pop1
        g1, g2 ← select two strings for
            reproduction.
For the selection of two strings roulette wheel is
implemented as follows:
(i) r = random() * sum_of_fitness
    [Hint: random() function returns a random
    number between 0 and 1]
(ii) psum = 0, i=0, m → size of the population
(iii) p → contains the population strings
(iv) psum = psum + p(i)
(v) i = i + 1
(vi) if ( i <= m) and (psum < r)) Goto Step: (iv)
(vii) return i

g3, g4 ← new strings after cross over.
g5, g6 ← strings after mutation, here a random
bit in the kernel is flopped or flopped.

Pop2(p) ← g5; p ← p+1; Pop2(p) ← g6;
end
min ← Min(Pop2); Pop1 ← Pop2;
pos ← where the B(i,j) = min;
end

```

---

### 4.3 Identification of Nipple Position using Ant Colony Optimization

Ant Colony Optimization (ACO) is a population-based approach first designed by Marco Dorigo and coworkers [17] and inspired by the foraging behavior of ant colonies. Individual ants are simple insects with limited memory and capable of performing simple actions. However, the

collective behavior of ants provides intelligent solutions to problems such as finding the shortest paths from the nest to a food source. Ants foraging for food lay down quantities of a volatile chemical substance named pheromone, marking their path that it follows. Ants smell pheromone and decide to follow the path with a high probability and thereby reinforce it with a further quantity of pheromone. The probability that an ant chooses a path increases with the number of ants choosing the path at previous times and with the strength of the pheromone concentration laid on it [1,38].

Similar to GA, the breast is divided into three regions [44]. The border pixels in the second region are extracted. For each kernel in the border pixel, calculate the posterior energy function value  $U(x)$ . [Kernel is a 3×3 window of neighborhood pixels]

$$U(x) = \{ \sum [(y - \mu)^2 / (2 * \sigma^2)] + \sum \log(\sigma) + \sum V(x) \} \quad (12)$$

where,  $y$  is the intensity value of pixels in the kernel,  $\mu$  is the mean value of the kernel,  $\sigma$  is the standard deviation of the kernel,  $V$  is the potential function of the kernel, and  $x$  is the label of the pixel. If  $x_1$  is equal to  $x_2$  in a kernel, then  $V(x) = \beta$ , otherwise 0, where  $\beta$  is visibility relative parameter ( $\beta \geq 0$ ). The MAP probability estimate can be written as:  $P(x|y) = \exp(-U(x))$ , the challenge of finding the MAP estimate of the segmentation is search for the optimum label which minimizes the posterior energy function  $U(x)$ . The goal of this method is to find out a pixel of the image on the border that maximizes the posterior energy function value. Initially assign the values for number of iterations (N), number of ants (K), initial pheromone value ( $T_0$ ), a constant value for pheromone update ( $\rho$ ). [Hint: N=50, K=10,  $T_0=0.001$  and  $\rho=0.9$ ].

#### **Pheromone Initialization:**

For each ant assign the initial pheromone value  $T_0$ . And for each ant select a random pixel from the border pixels set which has not been selected previously. A flag value is assigned for each pixel to know whether the pixels are selected or not. Initially the flag value is assigned as 0, once the pixel is selected the flag is changed to 1. This procedure is followed for all the ants. For each ant a separate column for pheromone and flag values are allocated in the solution matrix.

#### **Local Pheromone Update:**

Update the pheromone values for all the randomly selected pixels using the following equation:

$$T_{\text{new}} = (1 - \rho) * T_{\text{old}} + \rho * T_0, \quad (13)$$

where  $T_{\text{old}}$  and  $T_{\text{new}}$  are the old and new pheromone values, and  $\rho$  is rate of pheromone evaporation

parameter in local update, ranges from  $[0,1]$  i.e.,  $0 < \rho < 1$ . Calculate the posterior energy function value for all the selected pixels by the ants from the solution matrix.

#### Global Pheromone Update:

Compare the posterior energy function value for all the selected pixels from each ants, select the maximum value from the set, which is known as 'Local Maximum' (Lmax) or 'Iterations best' solution. This value is again compared with the 'Global Maximum' (Gmax). If local maximum is greater than global maximum, then the global maximum is assigned with the current local maximum. Then the ant, which generates this local maximum value, is selected and whose pheromone is updated using the following equation:

$$T_{new} = (1 - \alpha) * T_{old} + \alpha * \Delta T_{old}, \quad (14)$$

where  $T_{old}$  and  $T_{new}$  are the old and new pheromone values, and  $\alpha$  is rate of pheromone evaporation parameter in global update called as track's relative importance, ranges from  $[0,1]$  i.e.,  $0 < \alpha < 1$ , and  $\Delta$  is equal to  $(1 / Gmax)$ . For the remaining ants their pheromone is updated as:

$$T_{new} = (1 - \alpha) * T_{old}, \quad (15)$$

here, the  $\Delta$  is assumed as 0. Thus the pheromones are updated globally. The ant, which generates the Gmax, is traced and the corresponding pixel and its co-ordinates are stored. This procedure is repeated for all the image pixels. The entire procedure can be repeated for N number of times. At the final iteration, the co-ordinate of the image pixel that maximizes the posterior energy function value is considered as nipple position. Figure 7 shows the nipple position of a mammogram, detected by ant colony optimization algorithm.

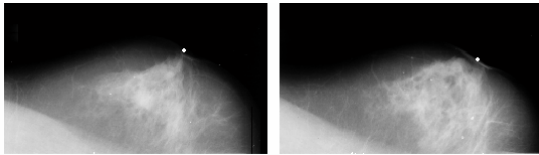


Figure 7. Nipple Identification using ACO

**Comparative Study:** The nipple position identified by the Ant Colony Optimization is compared with other methods. The points with values of 0-50 pixels of distance between the real position and the position obtained with the maximum height method have shorter distances between the real position and the position obtained with the second derivative method is 0-30 pixels. In case of average intensity gradient

method the difference is reduced to 0-15 pixels. The genetic algorithm approach has the difference of 0-10 pixels. Whereas the proposed ant colony optimization algorithm shorter the distance between the real position and the position obtained is 0-5 pixels. The proposed algorithm is as follows:

#### Algorithm: Identification of Nipple Position using Ant Colony Optimization:

---

```

Mij ← Original Image
Bij ← Border pixels
[m n] ← size of Bij
for each border pixel in Bij
    G ← kernel of the border pixel of size
        3×3 from M
    U ← fitness value; the posterior energy U
        (x) is calculated.
U(x) = {Σ[(y-μ)2/(2*σ2)] + Σ log(σ) + Σ V(x)}
end
N ← 50 - Number of iterations
K ← 10 - Number of Ants
T0 ← 0.001 - Initial pheromone value
ρ ← 0.9 - rate of pheromone evaporation
parameter
S ← {U(x), T0, flag} flag column mentions
whether the pixels is selected by the ant or
not.
Store the energy function values in S. Initialize all
the pheromone values with T0=0.001.
repeat for N times
    for each pixel in Mij
        for each ant
            gi ← a random border pixel for each ant,
                which is not selected previously.
            Tnew ← (1-ρ) * Told + ρ * T0 for gi
            end
            Lmax ← max(Ui(x))
            if (Lmax < Gmax) then Gmax = Lmax
            g ← Select the ant, whose solution is
                equal to local maximum
            Tnew ← (1 - α) * Told + α * ΔTold, only for g
            end

```

---

Trace the ant that generates the Gmax, from the ant's position find out the co-ordinates of the border pixel from the solution matrix. Consider this co-ordinate as nipple position.

**end**

## 5 Alignment Of Mammograms

Right and left breast images must be aligned prior to subtraction. Alignment involves the selection of reference points for transforming the coordinates of

one image in order to achieve correspondence between both images. In this study the right breast image is always transformed. The right mammogram is both displaced and rotated to align the images. The coordinates of the

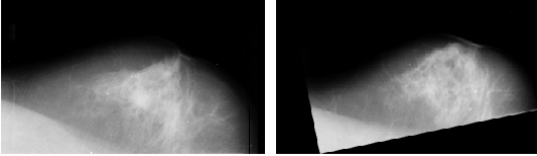


Figure 8. Alignment of Mammograms

detected nipples of both images determined the displacement. The coordinates of the points along the detected breast borders were used to determine the angle of rotation to achieve correspondence. After the right breast border was displaced, the correlation coefficient between the coordinates of the points of the left breast border and the coordinates of the points of the rotated right breast border was calculated for angles ranging between  $-5^\circ$  and  $5^\circ$  with one-degree step. The angle corresponding to the maximum value of the correlation coefficient was the angle of rotation of the right breast image, that is, the degrees that need to be rotated for the right breast border to match the left breast border. Figure 8 shows the left breast image and right breast image, which is transformed corresponding to left image.

### 5.1 Generating The Asymmetry Image

After the images were aligned, bilateral subtraction was performed [47,48] by subtracting the digital matrix of the left breast image from the digital matrix of the right breast image. Microcalcification in the right breast image have positive pixel values in the image obtained after subtraction, while microcalcification in the left breast image have negative pixel values in the subtracted image. As a result, two new images were generated: one with positive values and the other with negative values. The most common gray level was zero, which indicated no difference between the left and right images. Simple linear stretching of the two generated images to cover the entire available range of



Figure 9. Asymmetry Image

1024 gray levels was then calculated. The difference between corresponding pixels contains important information that can be used to discriminate between normal and abnormal tissue. The asymmetry image can be thresholded to extract suspicious regions. To generate FROC curve, the asymmetry image is thresholded using ten different intensity values ranges from 50-150. Figure 9 shows a asymmetry image and connected regions extracted based on thresholding to obtain a progressively larger number of high difference pixels.

## 6 Experiments And Results

Ultimately, the effectiveness of the proposed technique is determined by the extent to which potential abnormalities can be extracted from corresponding mammograms based on analysis of their asymmetry image. Figure 10 shows the normal left and right mammogram image. The Mammographic Image Analysis Society (MIAS) Database is used to evaluate the technique. This data is available at <ftp://peipa.essex.ac.uk>. The X-ray films in the database have been carefully selected from the United Kingdom National Breast Screening Programme and digitized with a Joyce-Lobel scanning microdensitometer to a resolution of  $50 \mu\text{m} \times 50 \mu\text{m}$ , 8 bits represent each pixel. The database contains 322 mammograms including normal, mass, and microcalcification cases. It indicates different classes of abnormalities such as calcification, well-defined circumscribed masses, speculated masses, ill-defined masses, architectural distortion, asymmetry and normal. Each of these abnormalities has been diagnosed and confirmed by a biopsy to indicate its severity: benign or malignant. Although the abnormalities vary greatly in shape, the ground truth is given as a center and radius of a circle, which encloses each abnormality.

All 161 MIAS image pairs were used in this

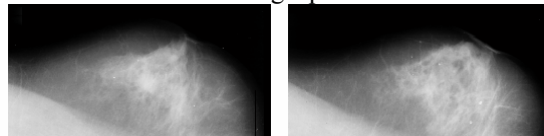


Figure 10. Left and Right Mammograms from MIAS dataset (a) mdb063 (b) mdb064

paper. A randomly selected set of 15 bilateral pairs drawn from the pairs with spiculated and circumscribed lesions was used for developing the algorithm and for guiding parameter setting. One of the training circumscribed cases also had an asymmetric density. The remaining abnormal and the normal image pairs were used to measure performance. Table 1 provides a list of different

categories of image pairs available in MIAS database. The true positive detection rate and the number of false positive detection rate at various thresholds of the asymmetry images are used to measure the algorithm's performance. These rates are represented using Free-Response Receiver Operating Characteristic (FROC) curves [31].

Table 1. Summary of MIAS bilateral image pairs

MIAS Category	No. of Image pairs	No. of Abnormalities
Normal	53	-
Circumscribed Masses	21	26
Spiculated Masses	19	19
Ill-defined Masses	14	15
Architectural Distortion	18	19
Asymmetry	14	14
Calcification	22	25
Total	161	118

True Positive (TP) and False Positive (FP) rates are calculated at 10 different thresholds selected on asymmetry image pixels to generate an FROC curve. A region extracted in the asymmetry image, which overlaps with a true abnormality as provided in the ground truth of the image, is called a true positive detection. An overlap means that at least 75% of the region extracted lies within the circle indicating a true abnormality as determined by MIAS database. For example, the mammogram mdb239.pgm, the spatial coordinate position of the suspicious region, x and y are 567, 808 respectively, and the radius is 25 pixels. The resultant asymmetry image contains the suspicious region at [567,807], with the radius of 25 pixels. Compared to the MIAS information on

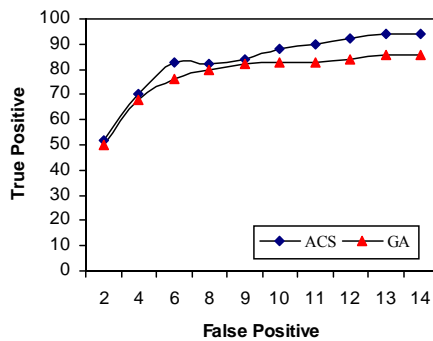


Figure 11. Combined results on all 161 normal and abnormal MIAS image pairs using ACO and GA

mdb239.pgm, results from the proposed method overlaps 98% of the specified region and this image is classified as true positive image. Suppose the overlap is less than 75% of the specified region, and then the image is considered as false positive image. In the previous methods such as Sallam and Bowyer [55], Lau and Bischof [41] have taken the overlap region of only 40% are considered as true positive. But in this paper, the true positive is considered only at 75% of overlap occurs. All other regions extracted by the algorithm are labeled as false positives. Figure 11 shows the FROC curves generated on the full test set, using 10 operating points. In general, it is expected that the true positive detection rate in an FROC curve will continue to increase or remain constant as the number of false positives increase. In this case the true positive rate actually drops at certain points. If the threshold value is low true detections may become merged with false positive regions.

The exact true positive and false positive rates are given in Table 2. The table also shows false positive rates for the set of 53 normal image pairs. As expected for the calcifications cases, the technique is only able to extract a very small fraction of the clusters. For the other abnormal categories (misc), best performance is achieved on ill-defined masses followed by circumscribed masses and asymmetry cases. The algorithm performance is slightly worse on spiculated lesions (spic) followed by architectural distortion pairs (arch). Unlike circumscribed and ill-defined masses, spiculated lesions and, to a larger extent, architectural distortion can have characteristic radiating or irregular thin structures without a distinct central mass.

Table 2. Detection Rates at different operating points using ACO

Operating Points	1	2	3	4	5	6	7	8	9	10
Misc TP	86.0	88.0	92.6	92.6	86.0	86.0	79.3	79.3	88.0	86.0
Misc FP	1.6	9.0	2.7	3.9	5.7	5.2	6.5	8.2	1.6	9.0
Circ TP	64.8	88.2	78.5	93.3	94.3	93.3	94.2	94.2	74.8	93.2
Circ FP	2.0	8.9	3.2	5.0	6.9	5.9	6.8	7.9	2.0	8.9
Asym TP	65.1	78.4	79.4	90.7	86.5	87.5	88.5	81.4	67.1	81.4
Asym FP	2.0	8.9	3.2	5.1	6.7	6.1	7.1	8.0	2.0	8.9
Spic TP	47.6	74.6	64.3	89.3	82.0	85.0	85.0	77.6	51.6	76.6
Spic FP	2.2	10.2	3.7	5.6	6.9	6.9	8.0	9.4	2.2	10.2
Arch TP	38.5	74.4	63.6	75.4	77.4	77.4	84.4	78.4	41.5	68.4
Arch FP	2.0	9.3	3.4	4.5	5.6	6.3	3.4	7.9	2.0	9.3
Total TP	59.2	82.3	75.5	88.5	85.6	83.6	76.5	84.0	63.2	85.3
Total FP	2.0	9.2	3.3	4.8	5.9	6.9	3.3	8.2	2.0	9.2
Calc TP	14.0	32.0	22.0	28.0	29.0	46.0	25.0	30.0	8.0	34.0
Calc FP	2.5	9.5	3.8	5.2	6.5	7.9	3.8	8.7	2.5	9.5
Norm FP	2.1	9.4	3.6	5.1	6.6	7.6	3.6	8.5	2.1	9.4

**Classification Ratio:** The area under the FROC curve ( $A_z$  value) is an important criterion for evaluating diagnostic performance [68,69]. The  $A_z$

value of FROC curve should be computed by normalizing the area under the FROC curve by the range of the abscissa. The value of  $A_z$  is 1.0 when the diagnostic detection has perfect performance, which means that TP rate is 100% and FP rate is 0%. The  $A_z$  value for the proposed algorithm is 0.94. The Table 3 shows the comparison of detection rate between the previous works and the proposed method.

**Table 3. Comparison of Detection Rate**

Authors & References	Methods	Detecti on Rate
Ferrari and Rangayyan [20]	Directional Filtering with Gabor wavelets	74.4%
Lau and Bischof [41]	Asymmetry Measures	85.0%
Sallam and Bowyer [55]	Unwarping Technique	86.6%
The proposed Approach	Genetic Algorithm Optimization	86.6%
	Ant Colony Optimization	94.8%

## 7 CONCLUSIONS

The proposed method has been designed to automatically detect both the breast border and nipple in digital mammograms using genetic operators and Ant Colony Optimization. The proposed algorithm is developed as an application using MATLAB v6.5 the figure 12 shows the layout and the outputs from the corresponding functions. Initially the mammogram images are smoothed by median filter and the pectoral muscle region is eliminated from the breast region. In border detection, the border pixel intensity values are considered as population strings, reproduction is applied to these strings to generate parent strings using fitness values, for crossover operator. Crossover and mutation operators are used to generate mated strings, the new population for detection of border. The detected border is evaluated using figure of merit, which shows the genetic algorithm detects exact border than other edge detectors. From the extracted border, the border pixels are considered as population strings to genetic algorithm and Ant Colony Optimization, to find out the optimum value from the border pixels. Ant Colony Optimization (ACO) algorithm updates the pheromones for each ants, while searching for the optimum value. At the final iteration, the border pixel, which returns the optimum value, is considered as the nipple position of the mammogram image.

The result of the nipple position using ACO is better than the results using highest peak method, second derivative method, average gradient method, and

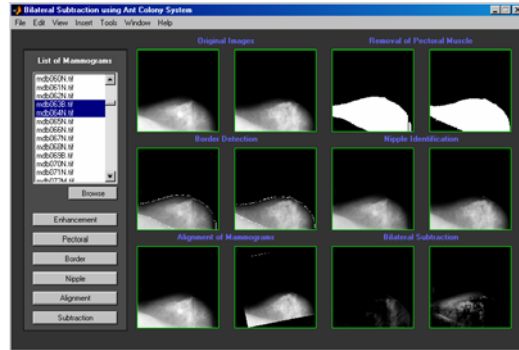


Figure 12. Screenshot from the implementation of Bilateral Subtraction using ACO. And developed by MATLAB v6.5

genetic algorithm comparatively. The border and nipple as references, the right mammogram is aligned corresponding to left mammogram, and left image is subtracted from right image to obtain the asymmetry image. Then the asymmetry image is thresholded to isolate the asymmetries or microcalcifications extracted from back ground tissue. To evaluate the performance of the proposed algorithm a FROC curve is generated. The experimental results shows that the proposed technique produces better  $A_z$  (0.94) results comparatively.

## REFERENCES

- [1] R. Beckers, J. L. Deneubourg, and S. Goss. Trails and U-turns in the selection of the shortest path by the ant *Lasius niger*. *J. Theor. Bio.*, 159:397–415, 1992.
- [2] J. E. Bell, P. R. McMullen. Ant colony optimization techniques for the vehicle routing problem, *Advanced Engineering Informatics*, 18:41-48, 2004.
- [3] U. Bick, M. Giger, R. Schmidt, D. Wolverton, and K. Doi, Computer-aided breast cancer detection in screening mammography. In *3rd Int. Workshop on Digital Mammography*, pp. 97–103. Elsevier, Amsterdam, 1996.
- [4] U. Bick, M.L. Giger, R.A. Schmidt, R.M. Nishikawa, D.E. Wolverton and K. Doi. Automated segmentation of digitized mammograms, *Acad. Radio.*, 2(1-9), 1995.
- [5] D. Brzakovic, N. Vujovic, V. Neskovic, P. Brzakovic, and B. Fogarty, B. Mammogram analysis by comparison with previous screenings. In *Proc. 2nd Int. Workshop on Digital Mammography*, 131–139, 1994.
- [6] R. Chandrasekhar and Y. Attikiouzel Y. A Simple Method for Automatically Locating the Nipple on Mammograms. *IEEE Transactions on Medical Imaging*, 16(5):483-494, 1998.
- [7] H. D. Cheng, J. Wang, and X. Shi. Microcalcification Detection Using Fuzzy Logic and Scale Space Approaches. *Pattern Recognition*, 37:363–375, 2004.
- [8] H. D. Cheng, X. Cai, X. W. Chen, L. Hu, and X. Lou, “Computer-Aided Detection and Classification of Microcalcifications in Mammograms: A Survey”, *Pattern Recognition*, pp: 2967–2991, v.36, 2003.

- [9] L. P. Clarke, M. Kallergi, W. Qian, H. D. Li, R. A. Clark, and M. L. Silbiger. Tree-structured non-linear filter and wavelet transform for microcalcification segmentation in digital mammography. *Cancer Lett.*, 77:173–181, 1994.
- [10] A. Colomi, M. Dorigo, and V. Maniezzo, In F.J. Varela, P. Bourguine. Distributed optimization by ant colonies. *Proceedings of the First European Conference on Artificial Life, Paris*, 1991.
- [11] S. Detounis. Computer-Aided Detection and Second Reading Utility and Implementation in a High-Volume Breast Clinic. *Applied Radiology*, 8-15, 2004.
- [12] A. P. Dhawan, Y. Chitre, C. Kaiser-Bonasso, and M. Moskowitz. Analysis of Mammographic MicroCalcificationifications Using Grey-Level Image Structure Features. *IEEE Transactions on Medical Imaging*, 15(3):246-259, 1996.
- [13] M. Dorigo, and G. Di Caro. The ant colony optimization meta-heuristic, In: D. Corne, M. Dorigo, F. Glover (Eds.), *New Ideas in Optimization*, McGraw-Hill, London, 11-32, 1999.
- [14] M. Dorigo, and G. Di Caro, L. M. Gambardella. Ant algorithms for discrete optimization. *Artificial Life*. 5:, 137–172, 1999.
- [15] M. Dorigo, G. Di Caro, and L. M. Gambardella. Ant algorithms for distributed discrete optimization. *Artificial Life*. 5:137–172, 1999.
- [16] M. Dorigo and L. M. Gambardella. Ant colonies for the traveling salesman problem. *BioSystems*, 43:73–81, 1997.
- [17] M. Dorigo, V. Maniezzo, and A. Colomi. Positive feed back as a search strategy. Technical Report 16 Politecnico di Milano, Italy, 1991.
- [18] M. Dorigo, V. Maniezzo, and A. Colomi. The Ant System: Optimization by a Colony of Cooperating Agents. *IEEE Transactions on Systems, Man and Cybernetics-Part B*, 1(26):29-41, 1996.
- [19] M. Dorigo and T. Stutzle. *Ant Colony Optimization*. Prentice Hall of India Pvt. Ltd., New Delhi, 2005.
- [20] R. J. Ferrari, R. M. Rangayyan, J. E. L. Desautels, and A. F. Frere. Analysis of Asymmetry in Mammograms via Directional Filtering With Gabor Wavelets. *IEEE Transactions On Medical Imaging*, 20(9):953 – 964, 2001.
- [21] R. J. Ferrari, R. M. Rangayyan, J. E. L. Desautels, R. A. Borges and A. F. Frere. Automatic Identification of the Pectoral Muscle in Mammograms. *IEEE Transactions On Medical Imaging*, 23(2):232-245, 2004.
- [22] Y. Ge, Q. C. Meng, C. J. Yan, J. Xu. A Hybrid Ant Colony Algorithm for Global Optimization of Continuous Multi-Extreme Functions. *Proceedings of the Third International Conference on Machine Learning and Cybernetics, Shanghai*, 2427-2432, 2004.
- [23] F. Glover. Tabu search: a tutorial. *Interfaces*, 20: 74–94, 1990.
- [24] D. E. Goldberg. *Genetic Algorithms in Search, Optimization, and Learning*. NY, Addison Wesley, 1989.
- [25] D. E. Goldberg. *Genetic Algorithms in Search, Optimization and Machine Learning*, Addison Wesley Longman Pte. Ltd., pp. 60-68, 3<sup>rd</sup> ed., 2000.
- [26] R. C. Gonzalez, R. E. Woods, and S. L. Eddins. *Digital Image Processing using MATLAB*. Pearson Edition, 2004.
- [27] S. Goss, S. Aron, J. L. Deneubourg, and J. M. Pasteels. Self-organized shortcuts in the Argentine ant. *Naturwissenschaften*, 76:579–581, 1989.
- [28] M. Gudmundsson, E. A. El-Kwae, and M. R. Kabuka. Edge Detection in Medical Images Using a Genetic Algorithm. *IEEE Transactions on Medical Imaging*, 17(3):469 – 474, 1998.
- [29] T. O. Gulsrud and J. H. Husoy. Optimal Filter-Based Detection of Microcalcifications. *IEEE Transactions on Biomedical Engineering*, 48(11):1272–1280, 2001.
- [30] W. Hand, J. L. Semmlow, L. V. Ackerman, and F. S. Alcorn, F. S. Computer screening of xero-mammograms: a technique for defining suspicious areas of the breast. *Comp. Biomed. Res.*, 12:445–460, 1979.
- [31] J. A. Hanley, and B. J. McNeil. The meaning and use of the area under a receiver operating characteristic (ROC), curve. *Radiology*, 143:29–36, 1982.
- [32] R. Haralick, and L. Shapiro, *Computer and Robot Vision*. Addison-Wesley, Reading, MA, 1992.
- [33] J. H. Holland. *Adaptation in Natural and Artificial Systems*. Ann Arbor: The University of Michigan, 1975.
- [34] A. K. Jain. *Fundamentals of Digital Image Processing*. Prentice Hall, 1989.
- [35] N. Karssemeijer, and G. M. te Brake, Combining single view features and asymmetry for detection of mass lesions. In *4th Int. Workshop on Digital Mammography*. Elsevier, Amsterdam, 1998.
- [36] C. Kimme, B. J. O’Loughlin, and J. Slansky, (1975) Automatic detection of suspicious abnormalities in breast radiographs. In *Proc. Conf. on Computer Graphics, Pattern Recognition and Data Structure*, 84–88, 1975.
- [37] S. Kirkpatrick, D. Gelatt, and M. P. Vecchi. Optimization by simulated annealing. 220: 671–680, 1983.
- [38] S. M. Kwok, R. Chandrasekhar, Y. Attikiouzel Y, and M. T. Rickard. Automatic Pectoral Muscle Segmentation on Mediolateral Oblique View Mammograms. *IEEE Transactions On Medical Imaging*, 23(9):1129-1140, 2004.
- [39] S. Lai, X. Li, and W. F. Bischof WF. On Techniques for Detecting Circumscribed Microcalcifications in Mammograms. *IEEE Transactions on Medical Imaging*, 8(4):377–386, 1989.
- [40] A.F. Laine, S. Schuler, J. Fan, and W. Huda, Mammographic feature enhancement by multiscale analysis, *IEEE Trans. Med. Imag.* 13(4):7250–7260, 1994.
- [41] T. K. Lau, and W. F. Bischof, Automated detection of breast tumors using the asymmetry approach. *Comp. Biomed. Res.*, 24:273–295, 1991.
- [42] H. Li, K. J. R. Liu, and S. C. B. Lo, Fractal modeling and segmentation for the enhancement of microcalcifications in digital mammograms, *IEEE Trans. Med. Imag.*, 16(6): 785–798, 1997.
- [43] H. Li, K. J. R. Liu, S. C. B. Lo, Fractal modeling of mammogram and enhancement of microcalcifications, *IEEE Nuclear Science Symposium & Medical Imaging Conference*, 3:1850–1854, 1996.
- [44] A. J. Mendez, P. G. Tahocesb, M. J. Lado, M. Souto, J. L. Correa, and J. J. Vidal. Automatic Detection of Breast Border and Nipple in Digital Mammograms. *Computer Methods and Programs in Biomedicine*, 49:253–262, 1996.
- [45] Z. Michalewicz. *Genetic Algorithms, Data Structures, Evolution Programs*. Heidelberg: Springer-Verlag, 3<sup>rd</sup> edition, 1996.
- [46] P. Miller, and S. Astley, Automated detection of mammographic asymmetry using anatomical features. *Int. J. Patt. Recogn. Artific. Intell.*, 7:1461–1476, 1993.
- [47] N. R. Mudigonda, R. M. Rangayyan, J. E. L. Desautels, Detection of Breast Masses in Mammograms by Density Slicing and Texture Flow-Field Analysis. *IEEE Transactions On Medical Imaging*, 20(12):1215-1227, 2001.
- [48] M. Muttarak, G. Peh, and B. Chaiwun. Malignant germ cell tumours of undescended testes: imaging features with

pathological correlation. *Clinical Radiology*, 59:198–204, 2004.

[49] S. Ouardfel and M. Batouche. MRF-based image segmentation using Ant Colony System. *Electronic Letters on Computer Vision and Image Analysis*, 2(2):12-24, 2003.

[50] C. A. Pena-Reyes, and M. Sipper. A fuzzy-genetic approach to breast cancer diagnosis. *Artificial Intelligence in Medicine*, 17:131-155, 1999.

[51] W. K. Pratt. *Digital Image Processing*. Wiley-Interscience Publication, 3<sup>rd</sup> edition, 2001.

[52] C. Priebe, R. Lorey, D. Marchette, and J. Solka. Nonparametric spatio-temporal change point analysis for early detection in mammography. In *2nd Int. Workshop on Digital Mammography*, Elsevier, Amsterdam, 111–120, 1994.

[53] W. Qian, L. P. Clarke, M. Kallergi, and R. A. Clark. Tree-Structured Nonlinear Filters in Digital Mammography. *IEEE Transactions on Medical Imaging*, 13(1):25-36, 1994.

[54] W. Qian, M. Kallergi, L. P. Clarke, H. D. Li, and P. Venugopal. Tree structured wavelet transform segmentation of microcalcifications in digital mammography. *Medical Physics*, 22(8):1247–1253, 1995.

[55] M. Y. Sallam and K. W. Bowyer. Registration and difference analysis of corresponding mammogram images. *Medical Image Analysis*, 3(2):103-118, 1999.

[56] L. Tabar, and P. B. Dean. The control of breast cancer through mammography screening. *Radiol. Clin. N. Am.* 25:961-973, 1987.

[57] K. Thangavel, M. Karnan, R. Siva Kumar, and A. Kaja Mohideen. Automatic Detection of Microcalcification in Mammograms—A Review. *International Journal on Graphics Vision and Image Processing*, 5, 2005. (Accepted)

[58] Thangavel Kuttiannan, and Karnan Marcus. Detection of Microcalcifications in Digital Mammograms using Genetic Algorithm. *Bio Informatics and Medical Engineering*, 6,2005. (Communicated)

[59] S. K. Wiles, J. M. Brady, and R. P. Highnam, Combining mammogram pairs in the detection of lesions. In *4th Int. Workshop on Digital Mammography*. Elsevier, Amsterdam, 1998.

[60] F. Winsberg, M. Elkin, J. Macy, V. Bordaz, and W. Weymouth. Detection of abnormalities in mammograms by means of optical scanning and computer analysis. *Radiology*, 89: 211–215, 1967.

[61] M. A. Wirth, A. Stapinski. Segmentation of the Breast Region in Mammograms Using Active Contours. Dept. of Computing and Information Science, University of Guelph.

[62] F. Yin, M. Giger, K. Doi, C. Metz, C. Vyborny, and R. Schmidt, Computerized detection of masses in digital mammograms: analysis of bilateral subtraction images. *Med. Phys.*, 18:955–963, 1991.

[63] F. Yin, M. Giger, K. Doi, C. Vyborny, and R. Schmidt, R. Computerized detection of masses in digital mammograms: Automated alignment of breast images and its effect on bilateral subtraction. *Med. Phys.*, 21:445–452, 1994.

[64] X. Zhou, and R. Gordon, Geometric unwarping of digital subtraction mammography. In *Proc. Vision Interface '88*, 25–30, 1998.

[65] W. Zouras, M. Giger, P. Lu, D. Wolverton, C. Vyborny, and K. Doi, Investigation of a temporal subtraction scheme for computerized detection of breast masses in mammograms. In *3rd Int. Workshop on Digital Mammography*, Elsevier, Amsterdam, 411–416, 1996.



About the Author—**THANGAVEL KUTTIANNAN**, received the Master of Science from Department of Mathematics, Bharathidasan University in 1986, and Master of Computer Applications Degree from Madurai Kamaraj University, India in 2001. He obtained his Ph. D. Degree from Mathematics department, Gandhigram Rural Institute-Deemed University in 1999. Currently he is working as Reader in Mathematics Department, Gandhigram Rural Institute-Deemed University, and his experience started from 1988; His area of interests includes medical image processing, artificial intelligence, neural network, and fuzzy logic.

About the Author—**KARNAN MARCUS**, received the Master of Computer Science and Engineering Degree from Computer Science and Engineering Department, Government College of Engineering, Manonmaniam Sundaranar University, Tamil Nadu, India, in 2000. Currently he is working as Assistant Professor, Department of Computer Science & Engineering, RVS College of Engineering & Technology, Tamil Nadu, India. And doing part-time research in the Department of computer Science and Applications, Gandhigram Rural Institute-Deemed University, Tamil Nadu, India. His area of interests includes medical image processing, artificial intelligence, neural network, genetic algorithm, pattern recognition and fuzzy logic.

The following author designated as corresponding author:  
**Name: Karnan Marcus, E-mail id: [karnanme@yahoo.com](mailto:karnanme@yahoo.com), [ktvel@rediffmail.com](mailto:ktvel@rediffmail.com)**  
**Postal Address: 153, Palayam, Palani, Dindigul Dt, Tamil Nadu, India – 624601.**  
**Fax.No:91-4551-227229,91-4551-227230,**  
**TELEPHONE.NO:91-4551-227229,91-4551-2272**